Atmospheric
Chemistry
and Physics

Agricultural ammonia emissions in China: reconciling bottom-up and top-down estimates

Lin Zhang[1], Youfan Chen[1], Yuanhong Zhao[1], Daven K. Henze[2], Liye Zhu[3], Yu Song[4], Fabien Paulot[5], Xuejun Liu[6], Yuepeng Pan[7], Yi Lin[8], and Binxiang Huang[9]

[1]Laboratory for Climate and Ocean–Atmosphere Studies, Department of Atmospheric and Oceanic Sciences,
School of Physics, Peking University, Beijing 100871, China
[2]Department of Mechanical Engineering, University of Colorado, Boulder, CO 80309, USA
[3]Department of Atmospheric and Oceanic Sciences, University of California, Los Angeles, CA 90095, USA
[4]State Key Joint Laboratory of Environmental Simulation and Pollution Control, Department of Environmental Science,
Peking University, Beijing 100871, China
[5]Program in Atmospheric and Oceanic Sciences, Princeton University, Princeton, NJ 08544, USA
[6]Key Laboratory of Plant–Soil Interactions of MOE, College of Resources and Environmental Sciences,
China Agricultural University, Beijing 100094, China
[7]State Key Laboratory of Atmospheric Boundary Layer Physics and Atmospheric Chemistry (LAPC),
Institute of Atmospheric Physics, Chinese Academy of Sciences, Beijing 100029, China
[8]School of Earth and Space Sciences, Peking University, Beijing 100871, China
[9]Department of Agrometeorology, College of Resources and Environmental Sciences, China Agricultural University,
Beijing 100193, China

Correspondence: Lin Zhang (zhanglg@pku.edu.cn)

Abstract. Current estimates of agricultural ammonia (NH_3) emissions in China differ by more than a factor of 2, hindering our understanding of their environmental consequences. Here we apply both bottom-up statistical and top-down inversion methods to quantify NH_3 emissions from agriculture in China for the year 2008. We first assimilate satellite observations of NH_3 column concentration from the Tropospheric Emission Spectrometer (TES) using the GEOS-Chem adjoint model to optimize Chinese anthropogenic NH_3 emissions at the $1/2° \times 2/3°$ horizontal resolution for March–October 2008. Optimized emissions show a strong summer peak, with emissions about 50 % higher in summer than spring and fall, which is underestimated in current bottom-up NH_3 emission estimates. To reconcile the latter with the top-down results, we revisit the processes of agricultural NH_3 emissions and develop an improved bottom-up inventory of Chinese NH_3 emissions from fertilizer application and livestock waste at the $1/2° \times 2/3°$ resolution. Our bottom-up emission inventory includes more detailed information on

crop-specific fertilizer application practices and better accounts for meteorological modulation of NH_3 emission factors in China. We find that annual anthropogenic NH_3 emissions are 11.7 Tg for 2008, with 5.05 Tg from fertilizer application and 5.31 Tg from livestock waste. The two sources together account for 88 % of total anthropogenic NH_3 emissions in China. Our bottom-up emission estimates also show a distinct seasonality peaking in summer, consistent with top-down results from the satellite-based inversion. Further evaluations using surface network measurements show that the model driven by our bottom-up emissions reproduces the observed spatial and seasonal variations of NH_3 gas concentrations and ammonium (NH_4^+) wet deposition fluxes over China well, providing additional credibility to the improvements we have made to our agricultural NH_3 emission inventory.

1　Introduction

Ammonia (NH_3) and its aerosol-phase product ammonium (NH_4^+) exert important influences on atmospheric chemistry and biodiversity. They contribute to formation of fine particulate matter (PM) that has adverse effects on air quality and visibility (Park et al., 2004; Lelieveld et al., 2015) and causes a cooling climatic forcing (Martin et al., 2004; Henze et al., 2012). Their deposition to nonagricultural ecosystems can further lead to soil acidification and eutrophication (Stevens et al., 2004; Bowman et al., 2008). Quantifying these environmental consequences requires accurate knowledge of NH_3 sources, which are mainly associated with agricultural farming and livestock production (Bouwman et al., 1997). China, due to its intensive agricultural activities, is one of the largest NH_3 emitting countries in the world. However, current estimates of Chinese agricultural NH_3 emissions differ by more than a factor of 2 (see Sect. 2). Here we aim to better constrain agricultural NH_3 emissions in China using available NH_3 concentration and wet deposition flux measurements interpreted by the GEOS-Chem chemical transport model (CTM) and its adjoint.

As the main alkaline gas in the atmosphere, NH_3 reacts with sulfuric acid (H_2SO_4) and nitric acid (HNO_3), which are produced by the oxidation of sulfur dioxide (SO_2) and nitrogen oxides (NO_x), to form ammonium sulfate and ammonium nitrate aerosols, respectively. These secondary inorganic aerosols account for 40–57 % of the fine PM concentrations in eastern China (Yang et al., 2011; Huang et al., 2014). Recent studies also highlighted the possible role of NH_3 in neutralizing aerosol pH that can strongly enhance formation of sulfate through heterogeneous oxidation of SO_2 (Wang et al., 2016; Cheng et al., 2016; Paulot et al., 2016). All this evidence leads to increasing concerns that the effectiveness of SO_2 and NO_x emission controls on fine PM pollution over China may be undermined by unregulated NH_3 emissions (Wang et al., 2013; Fu et al., 2017).

Emissions of NH_3 are generally estimated from bottom-up statistical methods or process-based models by considering activity data and emission factors (emissions per unit activity) of all possible sources. The two most important NH_3 sources are the application of synthetic fertilizers generated by the Haber–Bosch process (Erisman et al., 2008) and livestock production (volatilization of NH_3 from animal excreta). They together are estimated to contribute 57 % of global NH_3 emissions (Bouwman et al., 1997) and 80 % in Asia (Streets et al., 2003; Kurokawa et al., 2013). Bottom-up NH_3 emission estimates highly depend on the accuracy of activity data and emission factors that require detailed spatial and temporal information on local agricultural practices and environmental conditions as will be discussed in Sect. 2.

Inverse modeling methods provide top-down emission estimates through optimizing comparisons of model simulations with measurements (Gilliland et al., 2003, 2006; Pinder et al., 2006; Zhu et al., 2013; Paulot et al., 2014). Top-down estimates of NH_3 emissions over China have been rare due to limited concentration or flux measurements of reduced nitrogen (NH_x = gaseous NH_3 + aerosol NH_4^+). A previous inversion study by Paulot et al. (2014) used NH_4^+ wet deposition flux measurements from the Acid Deposition Monitoring Network in East Asia (EANET) that only included two sites in China over the study period. Satellite observations of atmospheric NH_3 concentration have been emerging in recent years. These satellite instruments include the Tropospheric Emission Spectrometer (TES) (Beer et al., 2008; Shephard et al., 2011), the Infrared Atmospheric Sounding Interferometer (IASI) (Clarisse et al., 2009; Van Damme et al., 2015), the Atmospheric Infrared Sounder (AIRS) (Warner et al., 2016, 2017), and the Cross-track Infrared Sounder (CrIS) (Shephard and Cady-Pereira, 2015), providing increasingly rich datasets to understand the spatial and temporal variability of NH_3 in the atmosphere.

In this study, we apply TES satellite observations of NH_3 column concentration to provide top-down constraints on NH_3 emissions in China for the year 2008 using the GEOS-Chem adjoint model at the $1/2° \times 2/3°$ horizontal resolution. In order to reconcile with the bottom-up estimates and to better understand inversion results, we construct a new bottom-up inventory of Chinese agricultural NH_3 emissions by using more practical fertilizer application rates and timing over different crop categories and by better considering the seasonal variability of emission factors. We further evaluate the top-down and the improved bottom-up Chinese NH_3 emissions using an ensemble of surface measurements of NH_3 gas concentration and NH_4^+ wet deposition flux.

2　Previous bottom-up estimates of Chinese NH_3 emissions

We summarize in Table 1 published bottom-up estimates of Chinese NH_3 emissions. Annual NH_3 emissions from fertilizer application, livestock waste, human excrement, and other sources (e.g., transportation, waste disposal, industry) are presented from each inventory. Total anthropogenic NH_3 emissions based on the years of 2005–2012 range from 8.4 to 18.3 teragram (Tg) NH_3 per annum (a^{-1}). The factor of 2 difference is not likely due to the different base years. Analyses of historical NH_3 emissions in China show relatively stable or weak increasing trends (less than 3 % yr^{-1}) since 2000 (Xu et al., 2016; Kang et al., 2016), consistent with trends in atmospheric NH_3 concentration observed from satellites (Warner et al., 2017; Fu et al., 2017).

Fertilizer application and livestock waste are the two largest NH_3 sources, together accounting for more than 82 % of the total anthropogenic emissions over China (Table 1). However, considerable differences exist in their emission totals and relative importance. Estimates of NH_3 emissions from fertilizer application in China range from 1.82 $Tg\,a^{-1}$ in 2004 (Li and Li, 2012) to 9.82 $Tg\,a^{-1}$ in 2010 (Zhao et al.,

Table 1. Bottom-up estimates of ammonia anthropogenic emissions in China[1].

References	Base year	Fertilizer application	Livestock waste	Human	Others[2]	Total
Yan et al. (2003)	1995	4.32	2.48[3]	0.21		7.01
Streets et al. (2003)	2000	6.8	5.17	1.63		13.6
Li and Li (2012)	2004	1.82	8.30	1.67	0.21	12.0
Wang et al. (2009)	2005	4.3	8.82	0.26		13.38
Zhang et al. (2011)	2005	4.31				
Dong et al. (2010)	2006	8.68	6.61	0.65	0.14	16.08
Huang et al. (2012)	2006	3.2	5.3	0.2	1.1	9.8
Cao et al. (2010)	2007	3.62	9.58		2.8	16.0
EDGAR	2008	8.1	3.1	0.1		11.3
Xu et al. (2016)	2008	3.3	3.8[3]	0.7	0.6	8.4
Paulot et al. (2014) (MASAGE)	2008	3.6	5.8	0.8		10.2
Kurokawa et al. (2013) (REAS v2)	2008	9.46	2.88	1.81	0.85	15.0
Zhao et al. (2013)	2010	9.82	7.36	1.12		18.3
Fu et al. (2015)	2011	3				
Kang et al. (2016)	2012	2.8	4.99	0.12	1.71	9.62
This study	2008	5.05	5.31	1.30[4]		11.7

[1] Emission totals in unit of $Tg\,NH_3\,a^{-1}$. [2] Others include sources from transportation, industry, waste disposal, and agricultural burning. [3] Only considering NH_3 emission from livestock manure spreading to cropland. [4] Emission estimates adopted from Huang et al. (2012).

2013). All these emission estimates are calculated by multiplying fertilizer use amounts with corresponding volatilization rates (emission factors), except for Fu et al. (2015) that considered bi-directional NH_3 fluxes over an agricultural model. Large differences are mainly due to uncertainties in NH_3 emission factors that are highly sensitive to fertilizer types, local soil, and meteorological properties (Bouwman et al., 2002; Søgaard et al., 2002). NH_3 emissions from livestock waste also range from 2.88 to $8.82\,Tg\,a^{-1}$. An important uncertainty is also attributed to emission factors from livestock waste that heavily relied on European-based measurements in earlier estimates (Streets et al., 2003). Moreover, some estimates, e.g., Yan et al. (2003) ($2.48\,Tg\,a^{-1}$ for 1995) and Xu et al. (2016) ($3.8\,Tg\,a^{-1}$ for 2008), only accounted for livestock manure spreading to cropland and omitted contributions from animal housing and manure storage.

NH_3 from humans, including latrines and human perspiration and respiration, is another source with considerable differences (0.12–$1.81\,Tg\,a^{-1}$). The major component of this source is from rural excrement stored in roughly constructed latrines without sewage service, with uncertainties in estimates of rural population and the associated NH_3 emission factor. Other sources, such as agricultural burning, transportation, waste disposal, and industry also contribute 0.14–$2.8\,Tg\,NH_3\,a^{-1}$, depending on inclusions of different source sectors in the emission inventories. For example, Dong et al. (2010) ($0.14\,Tg\,a^{-1}$) only estimated NH_3 emitted from the chemical industry. These sources are relatively small compared to agricultural sources of fertilizer ap-

plication and livestock waste at the national scale; however, recent studies show that fuel combustion, (Pan et al., 2016), transportation (Chang et al., 2016; Sun et al., 2017), or local green space (Teng et al., 2017) can be dominant sources of NH_3 in the urban atmosphere.

We find substantial differences in spatial and seasonal variations of NH_3 emissions among the inventories. Figure 1 compares spatial distributions of anthropogenic NH_3 emissions in China from four commonly used inventories: the Regional Emission in Asia (REAS v2) inventory (Kurokawa et al., 2013), the Streets et al. (2003) inventory, the Huang et al. (2012) inventory, and the Emission Database for Global Atmospheric Research (EDGAR) (Olivier and Berdowski, 2001). Although they all show higher NH_3 emission rates in the east than the west, with the highest emissions occurring over North China, there are distinct regional differences of 50–200 %. In particular, EDGAR shows much more evenly distributed NH_3 emission rates spreading over China than the other three inventories.

Figure 1 also shows seasonal variations in these Chinese NH_3 emissions. Some inventories such as EDGAR and REAS v2 do not consider the seasonality of NH_3 emissions due to a lack of reliable information. More recent estimates account for information on the timing of fertilizer application and influences of meteorology on NH_3 emission factors. We can see that Huang et al. (2012) suggest a weak summer peak in Chinese NH_3 emissions, while the MASAGE inventory (Paulot et al., 2014) indicates largest emissions in April and July. NH_3 emission estimates of Streets et al. (2003) have a strong peak in June and are much higher than Huang
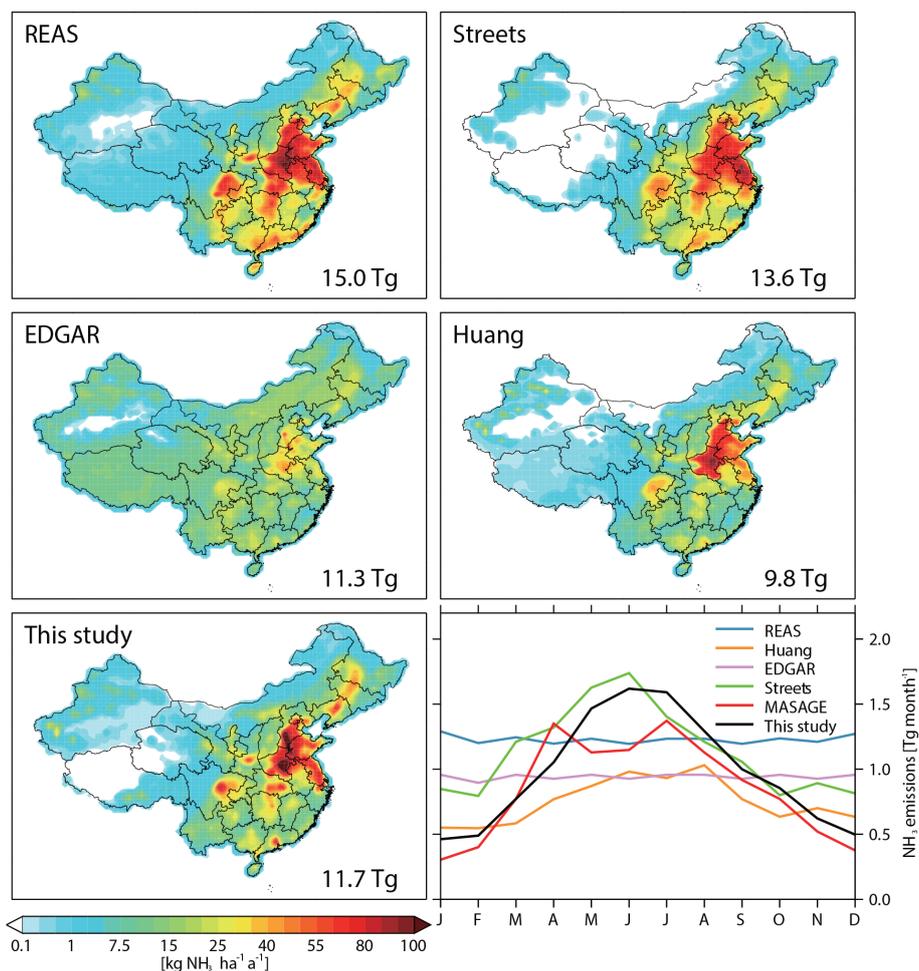
Figure 1. Spatial and seasonal variations of anthropogenic NH_3 emissions in China from different bottom-up inventories. Numbers inset are annual totals of Chinese anthropogenic NH_3 emissions. See Table 1 for references of the emission inventories.

et al. (2012) and Paulot et al. (2014) in winter. All these discrepancies as discussed above emphasize the need to improve our understanding of Chinese NH_3 emissions in light of measurements of NH_3 gas concentration and deposition flux.

3 Model description

3.1 The GEOS-Chem model

Here we will use the GEOS-Chem CTM and its adjoint to simulate the sources and sinks of NH_3 over China. GEOS-Chem is a global 3-D tropospheric chemistry model (http://geos-chem.org) driven by assimilated meteorological data from the Goddard Earth Observing System (GEOS) of the NASA Global Modeling and Assimilation Office (GMAO). The GEOS-5 meteorological data have a horizontal resolution of $1/2°$ latitude $\times 2/3°$ longitude and a temporal resolution of 3 h (1 h for surface variables). We apply here a one-way nested-grid version of GEOS-Chem with the native $1/2° \times 2/3°$ horizontal resolution over East Asia (70–

140° E, 15–55° N) and $2° \times 2.5°$ over the rest of the world (Wang et al., 2004; Chen et al., 2009).

The model simulates a detailed tropospheric ozone–NO_x–hydrocarbon–aerosol chemistry as described by Park et al. (2004) and Mao et al. (2010). NH_3 in the atmosphere is partitioned to gas and aerosol phases based on the Regional Particulate Model Aerosol Reacting System (RPMARES) thermodynamic equilibrium model (Binkowski and Roselle, 2003). NH_3 is thermodynamically favored to combine with H_2SO_4 to form ammonium bisulfate and ammonium sulfate, and excessive NH_3 can react with HNO_3 to form ammonium nitrate. GEOS-Chem simulations of secondary inorganic aerosols (ammonium, sulfate, and nitrate) over China have been validated by Wang et al. (2013) and Li et al. (2016) recently; both show high sensitivity of simulated nitrate concentrations to NH_3 emissions. GEOS-Chem also includes the ISORROPIA II thermodynamic equilibrium model (Fountoukis and Nenes, 2007). We find that differences in simulated monthly NH_3 concentrations over China by the two

equilibrium models are less than 5 %, and RPMARES runs about 30 % faster in the GEOS-Chem adjoint.

The model wet deposition scheme is described by Liu et al. (2001) with updates from Amos et al. (2012) for soluble gases and Wang et al. (2011) for aerosols. It includes convective updraft scavenging as well as large-scale precipitation rainout and washout. Uptake of gaseous NH_3 is estimated following Henry's law in warm clouds ($T > 268$ K), using a retention efficiency of 0.05 in mixed-phase clouds ($248 < T < 268$ K) and zero efficiency in cold clouds ($T < 248$ K) (Wang et al., 2008), while aerosol NH_4^+ is fully incorporated in all clouds. Dry deposition calculation follows a standard resistance-in-series model as described by (Wesely, 1989) for gases and Zhang et al. (2001) for aerosols.

We use the EDGAR global anthropogenic emissions overwritten by regional emission inventories including the US EPA 2005 National Emissions Inventory (NEI-2005), the European Monitoring and Evaluation Programme (EMEP) emissions, and the Canada Criteria Air Contaminants (CAC) inventory. Asian anthropogenic emissions are from Zhang et al. (2009) except for NH_3 as described below. These global and regional inventories are scaled to the simulation year of 2008 using the energy statistics as implemented by van Donkelaar et al. (2008). For the prior NH_3 emissions, we use the REAS v2 emission inventory that does not consider any seasonal variation (Kurokawa et al., 2013) so that the inverted emission seasonality is solely from satellite observations. We also follow Zhu et al. (2013) and increase NH_3 emissions from fertilizer use and livestock by 90 % in the daytime and reduce them by 90 % at night to account for their diurnal variability. Natural sources of NH_3 and NO_x from biomass burning, soil, and lightning follow the settings of Zhao et al. (2015) and are relatively small over China ($0.56 \, \mathrm{Tg} \, NH_3 \, a^{-1}$; Zhao et al., 2017).

3.2 The GEOS-Chem adjoint

We use the adjoint of GEOS-Chem to optimize Chinese NH_3 emissions through assimilation of TES NH_3 column measurements as will be discussed in the next section. The model adjoint is first described by Henze et al. (2007) for aerosols and Kopacz et al. (2009) for carbon monoxide. It has been highly validated and applied in studies to analyze aerosol sensitivities and constrain aerosol sources in the United States (Henze et al., 2009; Zhu et al., 2013; Mao et al., 2015) and China (Kharol et al., 2013; Zhang et al., 2015, 2016; Qu et al., 2017).

The emission optimization is conducted by minimizing the cost function (J), defined as

$$J(\mathbf{x}) = (Y(\mathbf{x}) - \mathbf{y}_{\mathrm{obs}})^{\mathrm{T}} \mathbf{S}_e^{-1} (Y(\mathbf{x}) - \mathbf{y}_{\mathrm{obs}}) \\ + (\boldsymbol{\sigma} - 1)^{\mathrm{T}} \mathbf{S}_a^{-1} (\boldsymbol{\sigma} - 1), \quad (1)$$

where $\mathbf{y}_{\mathrm{obs}}$ is the vector of satellite observations, $\mathbf{x}$ is the vector of NH_3 emissions in the model, $Y(\mathbf{x})$ represents simulated NH_3 concentration for comparison with $\mathbf{y}_{\mathrm{obs}}$, $\mathbf{x}_a$ is

the vector of a priori emissions, $\boldsymbol{\sigma}$ is the vector of scaling factors ($\mathbf{x}/\mathbf{x}_a$) for optimizing, and $\mathbf{S}_a$ and $\mathbf{S}_e$ are the a priori and observational error covariance matrices, respectively. Zhu et al. (2013) have previously applied the adjoint inverse model assimilating TES NH_3 data to constrain US NH_3 emissions, and Paulot et al. (2014) used wet NH_x deposition data to constrain East Asian NH_3 emissions, both at a coarser $2° \times 2.5°$ model resolution.

The adjoint model computes the gradient of the cost function ($\nabla_x J$) numerically, and applies the quasi-Newton L-BFGS-B algorithm (Byrd et al., 1995) to minimize the cost function iteratively. It usually takes about 15 iterations to reach the convergence, identified as the iteration when the cost function decreases by less than 2 % relative to the prior one. To lower the computational expenses, we follow the approach of Paulot et al. (2014) and use an offline NH_x ($NH_3 + NH_4^+$) simulation for the adjoint inversion that only calculates the physical and chemical transformation of NH_x driven by hourly simulated sulfate and total nitrate ($HNO_3 + NO_3^-$) concentrations archived from the standard simulation (Sect. 3.1). This approach would induce errors by not accounting for changes in total nitrate concentrations when NH_3 emissions change (Paulot et al., 2014). We find that a 30 % increase of Asian NH_3 emissions would increase the total nitrate concentration by about 10 %, but deviations of NH_3 concentrations in the offline simulation from the standard simulation due to the NH_3 emission change are less than 3 % over China.

4 Adjoint inversion of Chinese NH_3 emissions with satellite observations

We use satellite observations of NH_3 column concentration over China retrieved from TES, a high spectral resolution Fourier transform infrared spectrometer aboard the NASA Aura satellite launched in July 2004 (Beer et al., 2006). TES observations have a spatial resolution of $5 \, \mathrm{km} \times 8 \, \mathrm{km}$ at nadir with a local crossing time of 01:30 and 13:30 LT and global coverage achieved every 16 days (Beer et al., 2008; Shephard et al., 2011). TES retrievals of atmospheric NH_3 concentration are estimated by the optimal estimation method as described in Shephard et al. (2011). We filter the TES NH_3 retrievals by only using daytime observations with degree of freedom for signal (DOFS) greater than 0.1. We also correct the positive biases (0.04–1.0 ppbv in the lower troposphere depending on the a priori profile type used in the retrieval) in TES NH_3 retrievals following Zhu et al. (2013). Available TES observations for assimilation then become very spatially sparse for a single month. We assemble TES observations over the years of 2005–2010 for better spatial data coverage. AIRS NH_3 observations over 2002–2015 show weak increasing trends ($2.27 \% \, \mathrm{yr}^{-1}$) over Chinese agricultural areas.

Figure 2 shows TES-observed NH_3 column concentrations with a footprint size of $5 \, \mathrm{km} \times 8 \, \mathrm{km}$ from March to
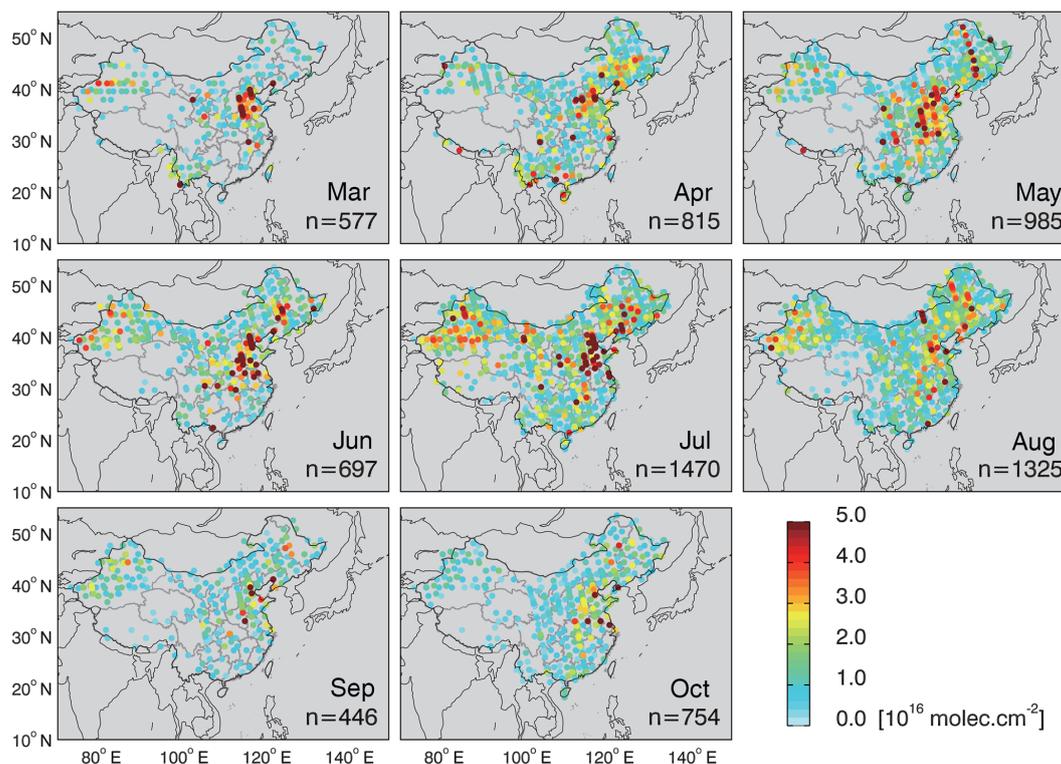
Figure 2. TES observations of NH$_3$ column concentration over China from March to October in the years 2005–2010. Each point represents a TES observation with a footprint resolution of 5 km × 8 km. Values inset are number (n) of valid observations for assimilation in each month.

October. We do not analyze the late fall and winter months (November–February) as the valid TES observations become very limited, which hinders a reliable emission inversion in those months. As can be seen in Fig. 2, the largest NH$_3$ column concentrations are observed over North China, reflecting intensive agricultural activities over this area. High NH$_3$ concentrations are also observed over the province of Xinjiang in Northwest China, which are likely emitted from animal grazing and remain mainly in gas phase due to lower NO$_x$ and SO$_2$ emissions to generate acids there. TES observations show a strong seasonality, with the national averaged NH$_3$ column concentration a factor of 2 higher in summer than spring, similar to other satellite NH$_3$ observations retrieved from AIRS (Warner et al., 2017) and IASI (Van Damme et al., 2015).

We now assimilate TES-observed NH$_3$ columns into the model through minimizing the cost function defined by Eq. (1). The emission optimization is conducted for each month of March–October 2008. Model results are sampled along the satellite orbits and then processed with TES a priori profiles and averaging kernel matrices as a necessary process for comparing with satellite retrievals based on the optimal estimation method (L. Zhang et al., 2010; Zhu et al., 2013). For the error covariance matrices, we assume the a priori error covariance (S$_a$) to be diagonal and the uncertainties to be

100 %. The observational error covariance (S$_{obs}$) is assumed to be 40 % of averaged values of observations and model results, accounting for uncertainties in both observations and the model. We have also conducted sensitivity inversions by using different S$_a$ (50 and 200 %) or S$_e$ (20 and 60 %) for the month of July.

Figure 3 shows differences between TES-observed and model-simulated NH$_3$ column concentrations with both the prior and optimized NH$_3$ emissions over China for April, July, and October. It also shows the correction ratios of optimized emissions over the prior emissions (REAS v2 in Fig. 1). We can see that with the prior Chinese NH$_3$ emissions, model results largely underestimate TES observations in July with a mean bias of −47 %, while they overestimate observations in April and October by 10–35 %. Model results with optimized NH$_3$ emissions improve comparison correlation coefficients (from 0.25–0.55 to 0.49–0.63) and significantly reduce the mean biases (−8–0 %). For these inversions, the cost functions are generally reduced by 35–45 %.

The emission correction ratios reflect seasonally and spatially heterogeneous adjustments. Ratios in July show overall increases over China by factors of 1.5–3 except for some locations over Northeast China. In April and October, there are large decreases (up to 70 %) over North China and Central China, while increases are noted in Southeast
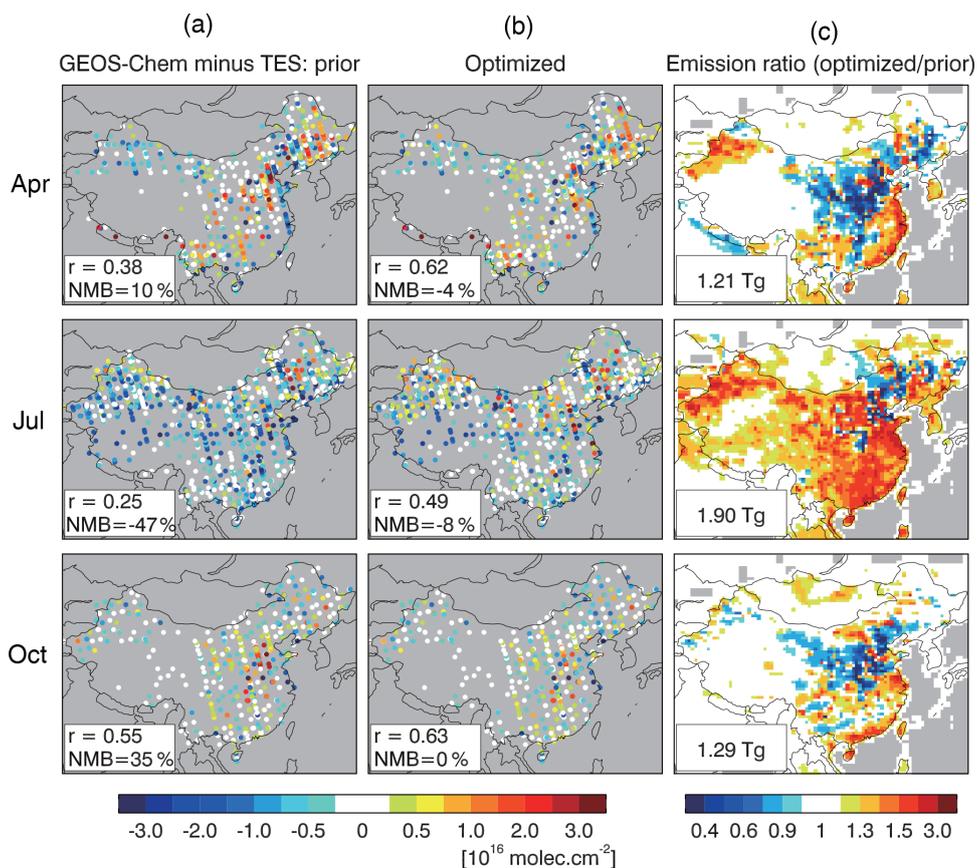
Figure 3. Differences between GEOS-Chem-simulated and TES-observed NH_3 column concentrations over China for April, July, and October. Panels **(a, b)** show results from model simulations with prior and optimized NH_3 emissions, respectively. Correlation coefficients (r) and normalized mean biases (NMB) are shown inset. Panel **(c)** shows monthly correction ratios relative to the prior emissions with optimized Chinese emission amounts shown inset.

China. Large emission increases are also shown over Northwest China in April and July. The optimized Chinese anthropogenic NH_3 emissions in July ($1.90\,\mathrm{Tg\,month^{-1}}$) are 47–57 % higher than April ($1.21\,\mathrm{Tg\,month^{-1}}$) and October ($1.29\,\mathrm{Tg\,month^{-1}}$). Inversion results for March–October indicate that Chinese NH_3 emissions peak in summer (see Fig. 7). Similar to previous work of Mao et al. (2015), we also find that the top-down results can be moderately affected by the selection of a priori and observational error covariance matrices. Sensitivity inversions with different S_a (50 and 200 %) or S_e (20 and 60 %) for July show a range of 1.60–$1.93\,\mathrm{Tg\,month^{-1}}$, with higher S_a and lower S_e values giving higher July emission estimates.

5   Improving bottom-up estimates of agricultural NH_3 emissions

The top-down estimates presented above show a stronger summer peak in Chinese NH_3 emissions than those represented in current bottom-up emission inventories (Fig. 1). Reconciling the discrepancy then requires us to better un-

derstand the bottom-up emissions from the underlying processes. Previous studies have shown that NH_3 emissions are highly sensitive to the magnitude and timing of fertilizer application as well as variations of meteorology (Søgaard et al., 2002; Gyldenkærne et al., 2005; Paulot et al., 2014), but these factors are neither sufficiently represented nor well evaluated in the Chinese NH_3 emission estimates. Here we construct an improved bottom-up Chinese NH_3 emission inventory from fertilizer application and livestock waste, with the objective to better estimate fertilizer application practices and emission factors. Figure 4 shows the schematic diagram of the bottom-up methodology as will be described in detail below.

5.1 NH_3 emission from fertilizer application

The MASAGE inventory recently developed by Paulot et al. (2014) provides spatial-resolved and crop-specific estimates of fertilizer application practices over the globe. We follow the methodology of MASAGE for NH_3 from fertilizer application but include detailed refinements for China. NH_3 emissions from fertilizer application (E_{NH_3-F}) are calculated as the product of synthetic fertilizer application mag-
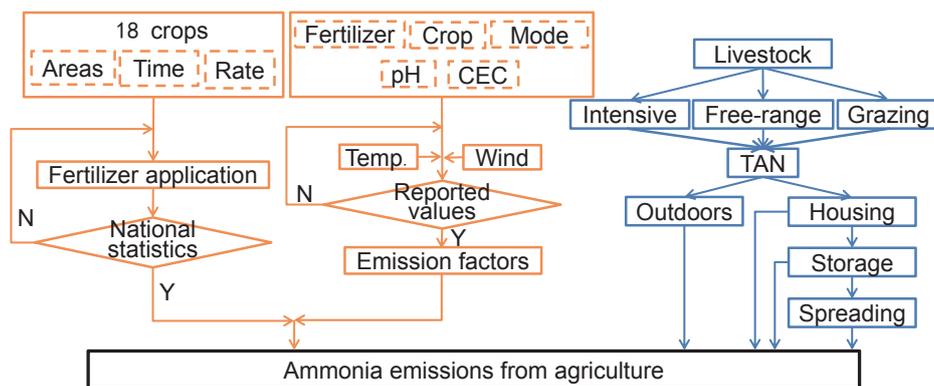
Figure 4. Schematic diagram for estimating agricultural NH$_3$ emissions from fertilizer application and livestock waste.

nitude (F) and corresponding emission factors (α_F):

$$E_{NH_3-F} = F \times \alpha_F. \tag{2}$$

5.1.1 Fertilizer application magnitude

We estimate fertilizer application amounts for 18 crop categories (including early/late rice, spring/winter wheat, spring/summer maize, cotton, potato, and others as shown in Fig. 5). The fertilizer application magnitude (F) is calculated as

$$F = \sum_c A_c \times \Psi_c(t), \tag{3}$$

where A_c is the planting area of crop c, and ψ represents fertilizer application rate at time t (day of the year). We use the EarthStat dataset of crop harvest area (Monfreda et al., 2008; EarthStat, 2015), which provides global crop harvest areas and yields at $5\,\text{min} \times 5\,\text{min}$ resolution for the year 2000. Here we regrid them to the model $1/2° \times 2/3°$ resolution, and scale the harvest area for each of the 18 crop categories to the year 2008 using the province-level data from the National Bureau of Statistics of China (NBSC, 2015). We use the harvest areas as the crop-planting areas except for rice and tobacco. Their planting areas are about 5 % of the harvest areas during the seeding period, and then they move to the transplanting fields till harvest.

Estimating the fertilizer application rate $\Psi_c(t)$ requires consideration of the planting schedule and fertilizer application practice for each crop. Paulot et al. (2014) distribute the annual fertilizer application amount over three stages (at planting, at growth, and after harvest) by assuming crop-specific application ratios. Here we consider much more detailed fertilizer application practices over China. Each crop requires the basal fertilizer applied at planting and several top dressing fertilizers during its growth (up to five application times). We construct tables of the fertilizer dates and rates (Tables S1 and S2 in the Supplement) for the main crop

categories in China based on Liao (1993) and Zhang and Zhang (2012). The timing of fertilizer application to each crop is based on its planting date or the calendar day (Table S1). We use the crop-planting dates of Sacks et al. (2010). Following Paulot et al. (2014), a Gaussian distribution function (Gyldenkærne et al., 2005) is applied to account for uncertainties and interannual variations of application dates:

$$F(t) = F \times \frac{1}{\sigma_c \sqrt{2\pi}} \times e^{\left(\frac{(t-\mu_c)^2}{-2\sigma_c^2}\right)}, \tag{4}$$

where μ_c is the crop-specific fertilizer application date, and σ_c is the deviation from the mean planting date estimated from the dataset of Sacks et al. (2010) as summarized in Table S1.

The procedures above allow us to estimate fertilizer application rates for each calendar day for the main crops listed in Tables S1 and S2, and we sum them up at the monthly scale. Fertilizers applied through the injection and broadcast modes are estimated separately. Based on fertilizer application practices, the first fertilizer application at plant is typically through injection (for rice and tobacco the first applications at both seeding and transplanting fields) and the rest by broadcast. For other crops, fruits, and vegetables, we use the annual fertilizer use amounts from the International Fertilizer Industry Association (IFA, 2013) and NBSC (2015), and then we distribute them spatially using the crop yield data of EarthStat (2015) and apply monthly variations proportional to the number of daylight hours following Park et al. (2004).

Figure 5 shows seasonal variations of fertilizer application to each crop category in China through injection and broadcast, separately. We estimate that $9.2\,\text{Tg N a}^{-1}$ fertilizers are used through injection and $15.8\,\text{Tg N a}^{-1}$ through broadcast. They show strong but different seasonal variations as resulted from variations of application timings for different crop categories. The use of injected fertilizers peaks in spring (April and May) and has a second peak in fall mainly due to winter wheat, while the use of broadcast fertilizers maximizes in late spring and summer. The annual total fertilizer applica-
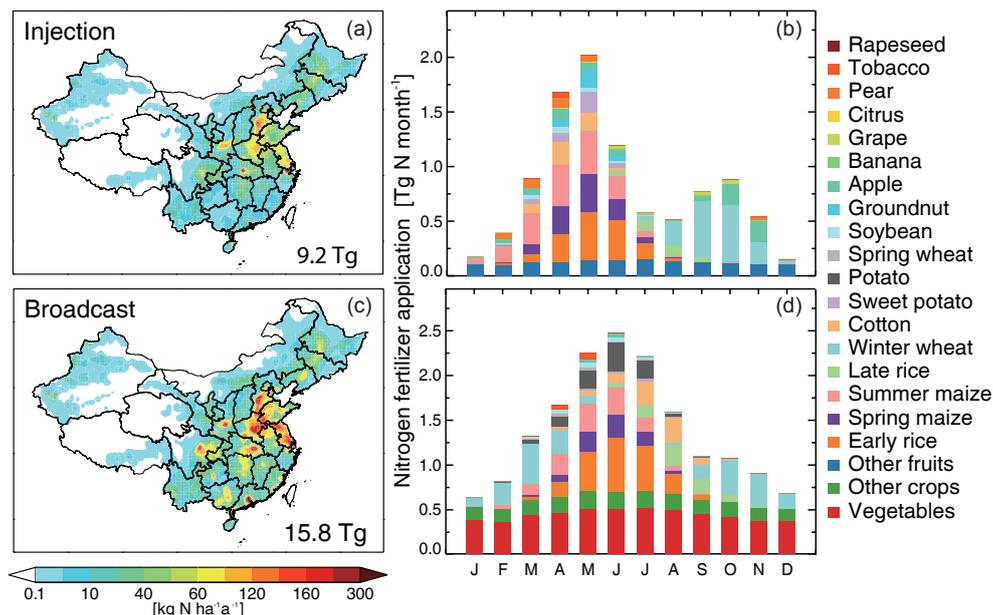
Figure 5. Fertilizer application through injection **(a, b)** and broadcast **(c, d)** techniques in China for 2008. Panels **(a, c)** show annual total fertilizer application at the $1/2° \times 2/3°$ model resolution with the annual totals given inset. Panels **(b, d)** show monthly fertilizer application amounts over China for the 18 crop types.
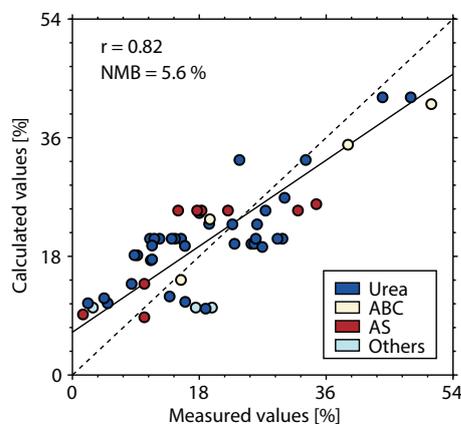
Figure 6. Comparison of calculated (using Eq. 5 in the text) and measured NH_3 emission factors from application of different fertilizers: urea, ammonium bicarbonate (ABC), ammonium sulfate (AS), and others in China. The correlation coefficient and normalized mean bias (NMB) are shown inset. Measurements of NH_3 emission factors are summarized in Table S4 in the Supplement.

tion is estimated to be 25.0 Tg N, compared with 22.4 Tg N in Huang et al. (2012) for 2006 and the FAO (Food and Agriculture Organization of the United Nations) estimate of 28.5 Tg N for 2008 (FAOSTAT, 2015).

5.1.2 Emission factor from fertilizer application

We estimate emission factors of NH_3 from fertilizer application as a function of soil properties and agricultural activity information and further modulated by meteorological conditions (Paulot et al., 2014). The emission factor is first calculated as

$$\alpha_0 = e^{f_{pH}+f_{CEC}+f_{type}+f_{crop}+f_{mode}}, \tag{5}$$

where the factors (f) represent effects of soil pH, cation exchange capacity (CEC), fertilizer type (e.g., urea, ammonium bicarbonate (ABC), ammonium sulfate (AS)), and application mode (broadcast and injection) on NH_3 volatilization mainly based on Bouwman et al. (2002) (Table S3 in the Supplement). Monthly scalars are then applied to account for the seasonality driven by meteorology:

$$\alpha_F = \alpha_0 \left(e^{0.0223T_i+0.0419W_i} \right) \Big/ \left(\frac{1}{12} \sum_{j=1}^{12} e^{0.0223T_j+0.0419W_j} \right), \tag{6}$$

where T_i and W_i are 2 m (meter) air temperature in °C and 10 m wind speed in m s^{-1} for month i, respectively (Søgaard et al., 2002; Gyldenkærne et al., 2005).

We use the gridded ($0.5° \times 0.5°$) soil pH data from the University of Wisconsin Nelson Institute Center for Sustainability and the Global Environment (SAGE, 2015), and the soil CEC data ($0.5° \times 0.5°$) from the ISRIC-World Soil Information (ISRIC WSI, 2015) of the World Data Center for Soils. Crop categories and application modes follow the calculation of fertilizer application rates as described
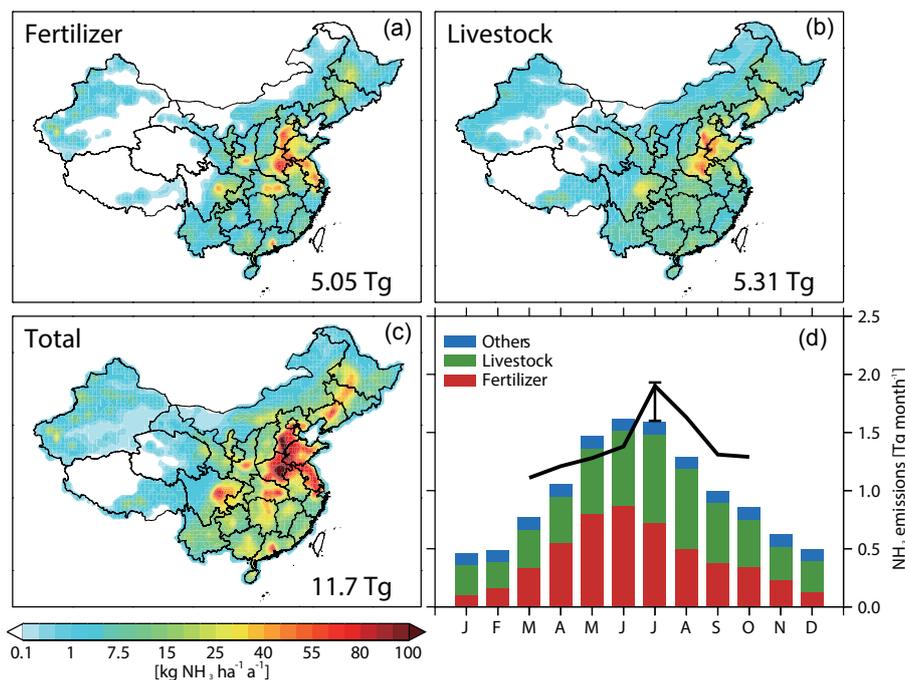
Figure 7. Improved bottom-up NH$_3$ emission estimates from fertilizer use **(a)**, livestock **(b)**, and total anthropogenic emissions **(c)** in China. Values inset are emission totals. Panel **(d)** shows seasonal variations in Chinese NH$_3$ emissions from different source categories. The bars represent our bottom-up estimates and the black line shows adjoint optimized anthropogenic totals for March–October. The vertical black line denotes the range of top-down estimates from inversions with different error configurations for the July month as described in the text.

above. Percentages of different fertilizer types applied to cropland are estimated based on the statistics from Zhang and Zhang (2012).

We have collected an ensemble of published measurements of NH$_3$ emission factors (volatilization rates) from fertilizer application that cover different regions of China and consider different fertilizer types and application modes, as summarized in Table S4 in the Supplement. We compare these measurements with corresponding emission factors derived by Eq. (5). This comparison does not include meteorological effects (Eq. 6) due to a lack of relevant measurements for the published emission factors. As shown in Fig. 6, calculated and measured values are in good agreement with a correlation coefficient of 0.80 and a mean bias of 10 %, supporting calculations of NH$_3$ emission factors using Eq. (5) for fertilizer application practices in China.

5.2   Livestock waste

The Chinese NH$_3$ emissions from livestock waste are commonly derived as the product of livestock population and emission factors (Streets et al., 2003; Paulot et al., 2014). Here we follow Huang et al. (2012) and Kang et al. (2016) that adopted a more process-based mass-flow approach by considering the transformation of nitrogen in animal husbandry. As shown in Fig. 4, a pool of total ammoniacal nitrogen (TAN) as input to manure management is estimated by

animal excreta from three main raising systems (free-range, intensive, and grazing). We use the gridded livestock (e.g., pork, beef, dairy, sheep, poultry) population from the Gridded Livestock of the World (GLW, 2015), and then we adjust them to match the province-level annual records of NBSC (2015) for 2008. The parameters of annual TAN excretion per animal considering both urine and feces and their nitrogen contents for each livestock category are given in Huang et al. (2012).

We estimate the content of TAN produced outdoors and indoors separately by assuming percentages of time spent outside and inside buildings for each livestock category (Huang et al., 2012). The outdoor TAN is directly deposited in the open air, while the indoor TAN can flow through the stages of housing, storage, and spreading to cropland as basal fertilizer with depletion of TAN from processes such as immobilization and leaching at each stage. NH$_3$ emissions from livestock are calculated as the product of TAN at the four stages and corresponding emission factors. We use the emission factors of Huang et al. (2012) and further account for the meteorological influences as represented by Eq. (6). We consider both air temperature and wind speed for outdoor NH$_3$ emissions, while we only account for air temperature for indoor emissions. Monthly emission factors are calculated using the GEOS-5 assimilated meteorological data at the model $1/2° × 2/3°$ resolution.
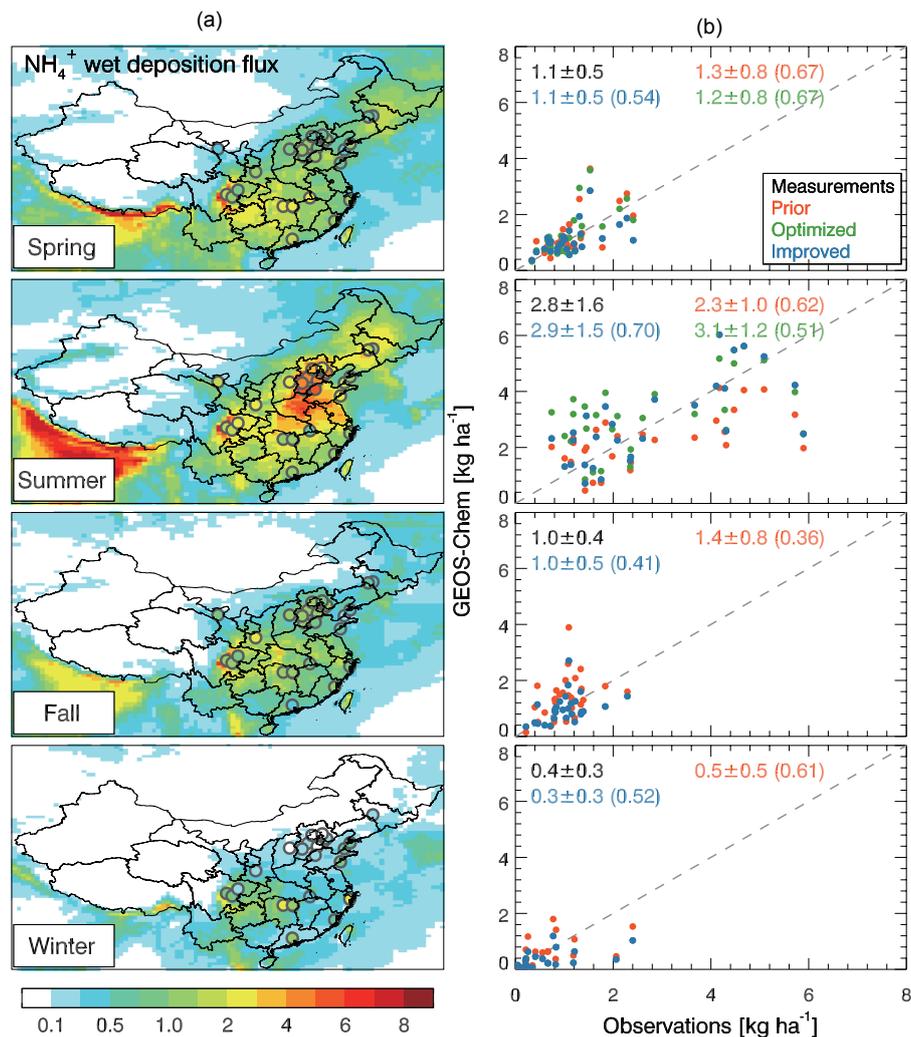
Figure 8. Comparison of simulated vs. measured seasonal mean NH_4^+ wet deposition fluxes over China. Spatial distributions **(a)** and scatterplots **(b)** are shown. Values inset are seasonal mean deposition fluxes and standard deviations for measurements (black), and model results with prior REAS v2 (orange), adjoint optimized (green; for spring and summer), and improved bottom-up (blue) NH_3 emissions. The correlation coefficients (values in parentheses) and the 1 : 1 line (dashed line) are also shown.

5.3 Improved emissions and evaluation with surface measurements

Figure 7 presents our improved bottom-up estimates of NH_3 emissions from fertilizer application, livestock waste, anthropogenic totals, and their seasonal variations. We adopt estimates of other NH_3 sources (agricultural burning, chemical industry, transportation, and waste disposal) from Huang et al. (2012) for calculating the total anthropogenic NH_3 emissions. Our bottom-up estimates show Chinese NH_3 emissions of $5.05 \, \text{Tg a}^{-1}$ from fertilizer application and $5.31 \, \text{Tg a}^{-1}$ from livestock and reach $11.7 \, \text{Tg a}^{-1}$ with the addition of other anthropogenic sources. High NH_3 emission rates occur over the North China Plain (over $80 \, \text{kg ha}^{-1} \, \text{a}^{-1}$ in parts of Hebei and Henan provinces) and the Sichuan Basin. Y. Zhang et al. (2010) also reported similar high NH_3

emission (with highest value up to $198 \, \text{kg ha}^{-1} \, \text{a}^{-1}$) in the North China Plain in the year 2004.

The spatial distribution and seasonal variations of our bottom-up NH_3 emission inventory are also presented in Fig. 1 for comparison with previous estimates. The regional distribution of our bottom-up estimates is broadly similar to Huang et al. (2012) and REAS v2 but exhibits some important regional differences. The total anthropogenic emission estimate of $11.7 \, \text{Tg a}^{-1}$ is in the middle of previous bottom-up estimates as summarized in Table 1; however, our NH_3 emissions show much more distinct seasonal variations than previous estimates (e.g., Streets et al., 2003), with emissions a factor of 3 higher in summer than winter. As shown in Fig. 7, this strong seasonality is consistent with the adjoint optimized emission totals for March–October (50 % higher in summer than spring and fall), considering uncertainties
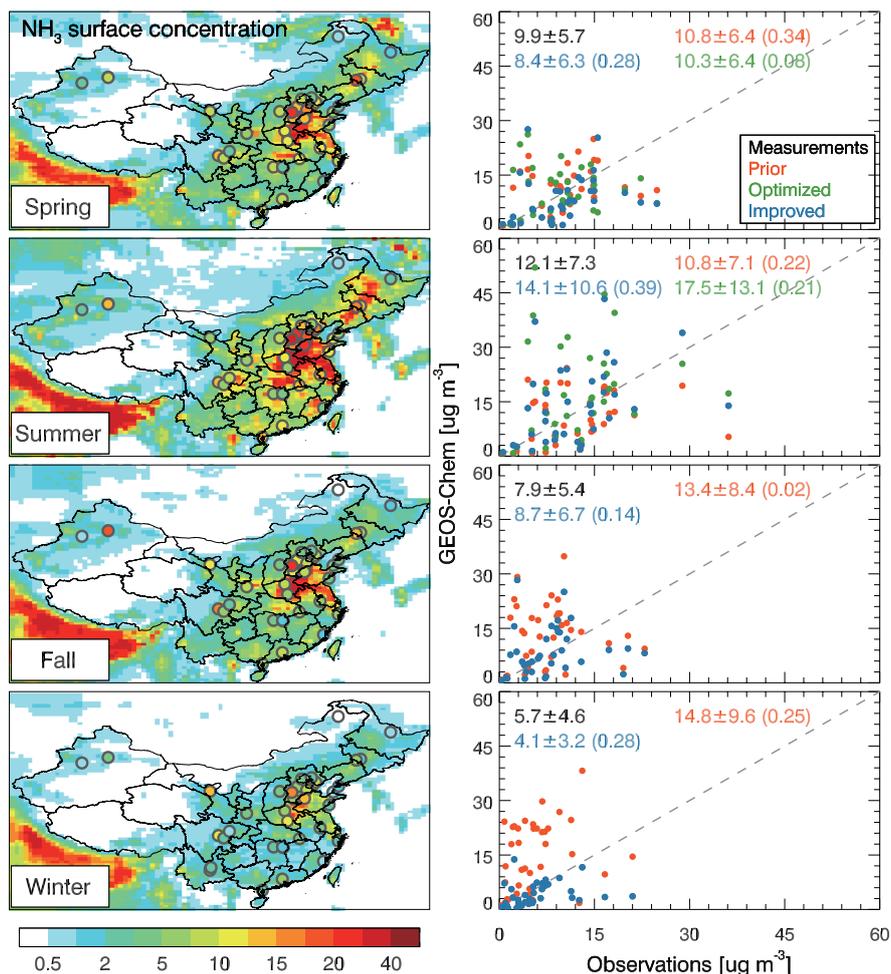
Figure 9. The same as Fig. 8, but for surface NH$_3$ concentration.

in the inversion results and satellite retrievals. The improved bottom-up Chinese NH$_3$ emissions are $\sim$ 15 % higher than the top-down estimates in May and June and $\sim$ 20 % lower in other months. This can also be seen from the comparison of simulated NH$_3$ columns using the improved bottom-up inventory with the TES measurements (Fig. S1 in the Supplement).

For further and independent evaluation of these NH$_3$ emissions, we use an ensemble of surface measurements of NH$_3$ gas concentration and NH$_4^+$ wet deposition flux compiled by Zhao et al. (2017). The dataset includes monthly averages from a nationwide measurement network over China for 2011–2012 (Xu et al., 2015), 10 sites in the North China Plain monitored by the Chinese Academy of Sciences for 2008–2010 (Pan et al., 2012), and two sites in China from EANET (2015). It should be noted that these measurements are compared with simulated results for 2008, inducing uncertainties from interannual variations. To test the influences from varying meteorology, we have conducted a model simulation over 2008–2012 with our improved bottom-up NH$_3$

emissions and other SO$_2$ and NO$_x$ anthropogenic emissions fixed to the year 2008 conditions. Our results show small differences in simulated seasonal mean NH$_4^+$ wet deposition fluxes and NH$_3$ gas concentrations between the 2008 and 5-year averaged model results except for the wintertime surface NH$_3$ concentrations for which the 2008 model results are 14 % lower (Figs. 8 and 9 as discussed below vs. Fig. S2 in the Supplement).

We show in Fig. 8 comparisons of NH$_4^+$ wet deposition flux measurements with model results using improved bottom-up, prior (REAS v2), and optimized Chinese NH$_3$ emissions. Measured NH$_4^+$ wet deposition fluxes indicate a strong peak in summer, with a national averaged monthly flux of 2.8 ± 1.6 kg ha^{-1} month^{-1} and a minimum in winter (0.4 ± 0.3 kg ha^{-1} month^{-1}). Part of this seasonality is driven by heavier precipitation in summer as model results with the prior REAS v2 emissions also capture some of the summer vs. winter deposition flux differences. However, model results with the prior REAS v2 still show underestimates of the flux measurements in summer and overesti-

mates in winter and spring, while the adjoint optimized NH_3 emissions reduce the model biases (e.g., mean biases reduced from 18 to 9 % in spring and from -18 to 11 % in summer). We can see that model results with our improved bottom-up NH_3 emissions reproduce the spatial and seasonal variations in measured NH_4^+ wet deposition fluxes well (correlation coefficients $r = 0.41$–0.70).

Figure 9 shows comparisons for the surface NH_3 gas concentration. Comparing model results with these surface concentration measurements requires addressing the inconsistency in the altitude they represent. The lowest model layer is centered at 70 m above surface, while all these Chinese surface sites used here measure at 3 m above surface. Zhang et al. (2012) previously quantified the vertical gradient of HNO_3 concentrations in the lowest model layer based on the dry deposition resistance-in-series formulation and the Monin–Obukhov similarity theorem. Here we follow the same approach to estimate the 3 m/70 m gradient of NH_3 concentrations driven by net NH_x flux in each grid. Implied NH_3 concentrations at 3 m are on average 20–30 % higher than those at 70 m. As a result, model results with our improved bottom-up emissions show better agreement (with seasonal mean biases within ± 20 %) with surface NH_3 concentration measurements than REAS v2 and optimized emissions. The relatively low correlation coefficients (0.14–0.39) may reflect difficulties for the model to fully capture the heterogeneity in NH_3 concentration due to its short lifetime, uncertainties gaseous NH_3 and aerosol NH_4^+ partitioning, and also interannual variations in NH_3 measurements. Furthermore, while land–atmosphere exchange of NH_3 is bidirectional, the model here treats it as one-way emission and dry deposition processes. Zhu et al. (2015) previously implemented a bi-directional NH_3 exchange algorithm in GEOS-Chem, and they found that it led to small changes in wet deposition fluxes but had large impacts on emission estimates and surface concentrations over eastern China. Future work is required to improve the bi-directional exchange processes in the model.

6   Conclusions

In summary, we have applied both bottom-up and top-down methods to better understand agricultural NH_3 emissions in China. A review of recent bottom-up estimates of Chinese NH_3 emissions shows substantial differences, not only in annual estimates of NH_3 emissions from fertilizer application and livestock waste, but also in their spatial and seasonal variations. The large differences mainly reflect limited information on fertilizer application practices and uncertainties in emission factors of NH_3 from agricultural activities.

We conduct top-down estimates of NH_3 emissions in China by assimilating TES satellite observations of NH_3 column concentration with the GEOS-Chem adjoint model for March–October 2008. The optimized Chinese NH_3 emis-

sions show a strong summer peak that is generally underestimated in current bottom-up emission estimates. Optimized monthly emissions in July are 1.90 Tg (1.60–1.93 Tg considering different configurations of error covariance), ~ 50 % higher than these in April (1.21 Tg) and October (1.29 Tg).

To interpret the top-down emission estimates, we revisit the bottom-up estimate of agricultural NH_3 emissions, aiming to better estimate the fertilizer application practices and NH_3 emission factors in China. We improve the emission inventory of Paulot et al. (2014) for NH_3 from fertilizer application with more realistic estimates of fertilizer use magnitudes and growth schedules of main crop categories in China. Emission factors of NH_3 from fertilizer application are calculated as a function of fertilizer type, application mode, soil property, and meteorological condition. Our validation of calculated values with an ensemble of published emission factor measurements shows a good agreement. For NH_3 emissions from livestock waste, we follow the mass-flow approach of Huang et al. (2012) and further account for meteorological influences (air temperature and wind speed) on NH_3 emission factors.

We find in our improved bottom-up inventory for the year 2008 that annual Chinese NH_3 emissions are 5.05 $\mathrm{Tg\,a^{-1}}$ from fertilizer application and 5.31 $\mathrm{Tg\,a^{-1}}$ from livestock waste. Addition of other anthropogenic NH_3 sources from Huang et al. (2012) (1.3 $\mathrm{Tg\,a^{-1}}$) suggests annual anthropogenic emissions of 11.7 $\mathrm{Tg\,a^{-1}}$. The improved bottom-up estimates of Chinese anthropogenic NH_3 emissions now display a strong seasonality, with emissions in summer ~ 50 % higher than spring and a factor of 3 higher than winter, similar to the seasonality in the top-down emission estimates.

We further evaluate the improved bottom-up and top-down Chinese NH_3 emissions using available surface measurements of NH_3 gas concentration and NH_4^+ wet deposition flux. We find that model results with improved bottom-up emissions reproduce the spatial and seasonal variations in these surface measurements well, demonstrating improvements in NH_3 emissions resulted from inclusion of detailed information on fertilizer application practices and seasonal variations of NH_3 emission factors. We acknowledge that measurements used in the study (both surface and TES satellite measurements) are still sparse in spatial coverage. Future studies using satellite NH_3 observations from AIRS, IASI, and CrIS that have better spatial data coverage will be valuable to constrain the spatial variability of NH_3 emissions.

References

Amos, H. M., Jacob, D. J., Holmes, C. D., Fisher, J. A., Wang, Q., Yantosca, R. M., Corbitt, E. S., Galarneau, E., Rutter, A. P., Gustin, M. S., Steffen, A., Schauer, J. J., Graydon, J. A., Louis, V. L. St., Talbot, R. W., Edgerton, E. S., Zhang, Y., and Sunderland, E. M.: Gas-particle partitioning of atmospheric Hg(II) and its effect on global mercury deposition, Atmos. Chem. Phys., 12, 591–603, https://doi.org/10.5194/acp-12-591-2012, 2012.

Beer, R.: TES on the Aura mission: scientific objectives, measurements, and analysis overview, IEEE T. Geosci. Remote, 44, 1102–1105, 2006.

Beer, R., Shephard, M. W., Kulawik, S. S., Clough, S. A., Eldering, A., Bowman, K. W., Sander, S. P., Fisher, B. M., Payne, V. H., Luo, M., Osterman, G. B., and Worden, J. R.: First satellite observations of lower tropospheric ammonia and methanol, Geophys. Res. Lett., 35, L09801, https://doi.org/10.1029/2008gl033642, 2008.

Binkowski, F. S. and Roselle, S. J.: Models-3 Community Multiscale Air Quality (CMAQ) model aerosol component 1. Model description, J. Geophys. Res., 108, 4183, https://doi.org/10.1029/2001JD001409, 2003.

Bouwman, A. F., Lee, D. S., Asman, W. A. H., Dentener, F. J., VanderHoek, K. W., and Olivier, J. G. J.: A global high-resolution emission inventory for ammonia, Global Biogeochem. Cy., 11, 561–587, 1997.

Bouwman, A. F., Boumans, L. J. M., and Batjes, N. H.: Estimation of global NH_3 volatilization loss from synthetic fertilizers and animal manure applied to arable lands and grasslands, Global Biogeochem. Cy., 16, 1024, https://doi.org/10.1029/2000GB001389, 2002.

Bowman, W. D., Cleveland, C. C., Halada, L., Hresko, J., and Baron, J. S.: Negative impact of nitrogen deposition on soil buffering capacity, Nat. Geosci., 1, 767–770, 2008.

Byrd, R. H., Lu, P. H., Nocedal, J., and Zhu, C. Y.: A limited memory algorithm for bound constrained optimization, SIAM J. Sci. Comput., 16, 1190–1208, 1995.

Cao, G. L., An, X. Q., Zhou, C. H., Ren, Y. Q., and Tu, J.: Emission inventory of air pollutants in China, China Environmental Science, 30, 900–906, 2010 (in Chinese with English abstract).

Chang, Y., Zou, Z., Deng, C., Huang, K., Collett, J. L., Lin, J., and Zhuang, G.: The importance of vehicle emissions as a source of atmospheric ammonia in the megacity of Shanghai, Atmos. Chem. Phys., 16, 3577–3594, https://doi.org/10.5194/acp-16-3577-2016, 2016.

Chen, D., Wang, Y., McElroy, M. B., He, K., Yantosca, R. M., and Le Sager, P.: Regional CO pollution and export in China simulated by the high-resolution nested-grid GEOS-Chem model, Atmos. Chem. Phys., 9, 3825–3839, https://doi.org/10.5194/acp-9-3825-2009, 2009.

Cheng, Y., Zheng, G., Wei, C., Mu, Q., Zheng, B., Wang, Z., Gao, M., Zhang, Q., He, K., Carmichael, G., Pöschl, U., and Su, H.: Reactive nitrogen chemistry in aerosol water as a source of sulfate during haze events in China, Sci. Adv., 2, e1601530, https://doi.org/10.1126/sciadv.1601530, 2016.

Clarisse, L., Clerbaux, C., Dentener, F., Hurtmans, D., and Coheur, P.-F.: Global ammonia distribution derived from infrared satellite observations, Nat. Geosci., 2, 479–483, 2009.

Dong, W. X., Xin, J., and Wang, S. X.: Temporal and spatial distribution of anthropogenic ammonia emissions in China: 1994–2006, Environ. Sci., 31, 1457–1463, 2010 (in Chinese with English abstract).

EANET: The Acid Deposition Monitoring Network in East Asia, available at: http://www.eanet.asia/index.html (last access: December 2015), 2015.

EarthStat: University of Minnesota's Institute on the Environment and the Ramankutty Lab at the University of British Columbia, Vancouver, available at: http://www.earthstat.org/ (last access: December 2015), 2015.

Erisman, J. W., Sutton, M. A., Galloway, J., Klimont, Z., and Winiwarter, W.: How a century of ammonia synthesis changed the world, Nat. Geosci., 1, 636–639, https://doi.org/10.1038/ngeo325, 2008.

FAOSTAT (Food and Agriculture Organization of the United Nations (FAO) Statistics Division): available at: http://www.fao.org/faostat/ (last access: December 2015), 2015.

Fountoukis, C. and Nenes, A.: ISORROPIA II: a computationally efficient thermodynamic equilibrium model for K^+–Ca^{2+}–Mg^{2+}–NH_4^+–Na^+–SO_4^{2-}–NO_3^-–Cl^-–H_2O aerosols, Atmos. Chem. Phys., 7, 4639–4659, https://doi.org/10.5194/acp-7-4639-2007, 2007.

Fu, X., Wang, S. X., Ran, L. M., Pleim, J. E., Cooter, E., Bash, J. O., Benson, V., and Hao, J. M.: Estimating NH_3 emissions from agricultural fertilizer application in China using the bi-directional CMAQ model coupled to an agro-ecosystem model, Atmos. Chem. Phys., 15, 6637–6649, https://doi.org/10.5194/acp-15-6637-2015, 2015.

Fu, X., Wang, S., Xing, J., Zhang, X., Wang, T., and Hao, J.: Increasing ammonia concentrations reduce the effectiveness of particle pollution control achieved via SO_2 and NO_x emissions re-

duction in East China, Environ. Sci. Technol. Lett., 4, 221–227, https://doi.org/10.1021/acs.estlett.7b00143, 2017.

Gilliland, A. B., Dennis, R. L., Roselle, S. J., and Pierce, T. E.: Seasonal NH_3 emission estimates for the eastern United States based on ammonium wet concentrations and an inverse modeling method, J. Geophys. Res., 108, 4477, https://doi.org/10.1029/2002jd003063, 2003.

Gilliland, A. B., Wyat Appel, K., Pinder, R. W., and Dennis, R. L.: Seasonal NH_3 emissions for the continental United States: inverse model estimation and evaluation, Atmos. Environ., 40, 4986–4998, 2006.

GLW (Gridded Livestock of the World): available at: http://www.fao.org/ag/againfo/resources/en/glw/home.html (last access: December 2015), 2015.

Gyldenkærne, S., Ambelas Skjøth, C., Hertel, O., and Ellermann, T.: A dynamical ammonia emission parameterization for use in air pollution models, J. Geophys. Res.-Atmos., 110, 1275–1287, https://doi.org/10.1029/2004jd005459, 2005.

Henze, D. K., Hakami, A., and Seinfeld, J. H.: Development of the adjoint of GEOS-Chem, Atmos. Chem. Phys., 7, 2413–2433, https://doi.org/10.5194/acp-7-2413-2007, 2007.

Henze, D. K., Seinfeld, J. H., and Shindell, D. T.: Inverse modeling and mapping US air quality influences of inorganic $PM_{2.5}$ precursor emissions using the adjoint of GEOS-Chem, Atmos. Chem. Phys., 9, 5877–5903, https://doi.org/10.5194/acp-9-5877-2009, 2009.

Henze, D. K., Shindell, D. T., Akhtar, F., Spurr, R. J. D., Pinder, R. W., Loughlin, D., Kopacz, M., Sing, K., and Shim, C.: Spatially refined aerosol direct radiative forcing efficiencies, Environ. Sci. Technol., 46, 9511–9518, https://doi.org/10.1021/es301993s, 2012.

Huang, X., Song, Y., Li, M. M., Li, J. F., Huo, Q., Cai, X. H., Zhu, T., Hu, M., and Zhang, H. S.: A high-resolution ammonia emission inventory in China, Global Biogeochem. Cy., 26, GB1030, https://doi.org/10.1029/2011GB004161, 2012.

Huang, R. J., Zhang, Y., Bozzetti, C., Ho, K. F., Cao, J. J., Han, Y., Daellenbach, K. R., Slowik, J. G., Platt, S. M., Canonaco, F., Zotter, P., Wolf, R., Pieber, S. M., Bruns, E. A., Crippa, M., Ciarelli, G., Piazzalunga, A., Schwikowski, M., Abbaszade, G., Schnelle-Kreis, J., Zimmermann, R., An, Z., Szidat, S., Baltensperger, U., El Haddad, I., and Prevot, A. S.: High secondary aerosol contribution to particulate pollution during haze events in China, Nature, 514, 218–222, https://doi.org/10.1038/nature13774, 2014.

IFA (International Fertilizer Industry Association): Assessment of Fertilizer Use by Crop at the Global Level, Paris, France, 2013.

ISRIC WSI (ISRIC-World Soil Information): available at: http://www.isric.org (last access: December 2015), 2015.

Kang, Y., Liu, M., Song, Y., Huang, X., Yao, H., Cai, X., Zhang, H., Kang, L., Liu, X., Yan, X., He, H., Zhang, Q., Shao, M., and Zhu, T.: High-resolution ammonia emissions inventories in China from 1980 to 2012, Atmos. Chem. Phys., 16, 2043–2058, https://doi.org/10.5194/acp-16-2043-2016, 2016.

Kharol, S. K., Martin, R. V., Philip, S., Vogel, S., Henze, D. K., Chen, D., Wang, Y., Zhang, Q., and Heald, C. L.: Persistent sensitivity of Asian aerosol to emissions of nitrogen oxides, Geophys. Res. Lett., 40, 1–6, https://doi.org/10.1002/grl.50234, 2013.

Kurokawa, J., Ohara, T., Morikawa, T., Hanayama, S., Janssens-Maenhout, G., Fukui, T., Kawashima, K., and Akimoto, H.: Emissions of air pollutants and greenhouse gases over Asian regions during 2000–2008: Regional Emission inventory in ASia (REAS) version 2, Atmos. Chem. Phys., 13, 11019–11058, https://doi.org/10.5194/acp-13-11019-2013, 2013.

Kopacz, M., Jacob, D. J., Henze, D. K., Heald, C. L., Streets, D. G., and Zhang, Q.: Comparison of adjoint and analytical Bayesian inversion methods for constraining Asian sources of carbon monoxide using satellite (MOPITT) measurements of CO columns, J. Geophys. Res.-Atmos., 114, D04305, https://doi.org/10.1029/2007JD009264, 2009.

Lelieveld, J., Evans, J. S., Fnais, M., Giannadaki, D., and Pozzer, A.: The contribution of outdoor air pollution sources to premature mortality on a global scale, Nature, 525, 367–371, https://doi.org/10.1038/nature15371, 2015.

Li, K., Liao, H., Zhu, J., and Moch, J.: Implications of RCP emissions on future $PM_{2.5}$ air quality and direct radiative forcing over China, J. Geophys. Res.-Atmos., 121, 12985–13008, https://doi.org/10.1002/2016JD025623, 2016.

Li, X. Y. and Li, H. P.: Emission and distribution of NH_3 and NO_x in China, China Environmental Science, 32, 37–42, 2012 (in Chinese with English abstract).

Liao, J.: Fertilizer Application and Analysis, Shanghai Science and Technology Press, Shanghai, 1993 (in Chinese).

Liu, H. Y., Jacob, D. J., Bey, I., and Yantosca, R. M.: Constraints from Pb-210 and Be-7 on wet deposition and transport in a global three-dimensional chemical tracer model driven by assimilated meteorological fields, J. Geophys. Res., 106, 12109–12128, 2001.

Mao, J., Jacob, D. J., Evans, M. J., Olson, J. R., Ren, X., Brune, W. H., Clair, J. M. St., Crounse, J. D., Spencer, K. M., Beaver, M. R., Wennberg, P. O., Cubison, M. J., Jimenez, J. L., Fried, A., Weibring, P., Walega, J. G., Hall, S. R., Weinheimer, A. J., Cohen, R. C., Chen, G., Crawford, J. H., McNaughton, C., Clarke, A. D., Jaeglé, L., Fisher, J. A., Yantosca, R. M., Le Sager, P., and Carouge, C.: Chemistry of hydrogen oxide radicals (HO_x) in the Arctic troposphere in spring, Atmos. Chem. Phys., 10, 5823–5838, https://doi.org/10.5194/acp-10-5823-2010, 2010.

Mao, Y. H., Li, Q. B., Henze, D. K., Jiang, Z., Jones, D. B. A., Kopacz, M., He, C., Qi, L., Gao, M., Hao, W.-M., and Liou, K.-N.: Estimates of black carbon emissions in the western United States using the GEOS-Chem adjoint model, Atmos. Chem. Phys., 15, 7685–7702, https://doi.org/10.5194/acp-15-7685-2015, 2015.

Martin, S. T., Hung, H.-M., Park, R. J., Jacob, D. J., Spurr, R. J. D., Chance, K. V., and Chin, M.: Effects of the physical state of tropospheric ammonium-sulfate-nitrate particles on global aerosol direct radiative forcing, Atmos. Chem. Phys., 4, 183–214, https://doi.org/10.5194/acp-4-183-2004, 2004.

Monfreda, C., Ramankutty, N., and Foley, J. A.: Farming the planet: 2. Geographic distribution of crop areas, yields, physiological types, and net primary production in the year 2000, Global Biogeochem. Cy., 22, GB1022, https://doi.org/10.1029/2007GB002947, 2008.

NBSC (National Bureau of Statistics of China): available at http://data.stats.gov.cn/ (last access: December 2015), 2015.

Olivier, J. G. J. and Berdowski, J. J. M.: Global emissions sources and sinks, in: The Climate System, edited by: Berdowski, J., Guicherit, R., and Heij, B. J., A. A. Balkema Publishers/Swets

and Zeitlinger Publishers, Lisse, the Netherlands, 33–78, ISBN: 9058092550, 2001.

Pan, Y., Tian, S., Liu, D., Fang, Y., Zhu, X., Zhang, Q., Zheng, B., Michalski, G., and Wang, Y.: Fossil fuel combustion-related emissions dominate atmospheric ammonia sources during severe haze episodes: evidence from ^{15}N-stable isotope in size-resolved aerosol ammonium, Environ. Sci. Technol, 50, 8049–8056, 2016.

Pan, Y. P., Wang, Y. S., Tang, G. Q., and Wu, D.: Wet and dry deposition of atmospheric nitrogen at ten sites in Northern China, Atmos. Chem. Phys., 12, 6515–6535, https://doi.org/10.5194/acp-12-6515-2012, 2012.

Park, R. J., Jacob, D. J., Field, B. D., Yantosca, R. M., and Chin, M.: Natural and transboundary pollution influences on sulfate-nitrate-ammonium aerosols in the United States: implications for policy, J. Geophys. Res.-Atmos., 109, D15204, https://doi.org/10.1029/2003jd004473, 2004.

Paulot, F., Jacob, D. J., Pinder, R. W., Bash, J. O., Travis, K., and Henze, D. K.: Ammonia emissions in the United States, European Union, and China derived by high-resolution inversion of ammonium wet deposition data: interpretation with a new agricultural emissions inventory (MASAGE_NH3), J. Geophys. Res.-Atmos., 119, 4343–4364, https://doi.org/10.1002/2013JD021130, 2014.

Paulot, F., Fan, S.-M., and Horowitz, L. W.: Contrasting seasonal responses of sulfate aerosols to declining SO$_2$ emissions in the eastern US: implications for the efficacy of SO$_2$ emission controls, Geophys. Res. Lett., 43, 455–464, https://doi.org/10.1002/2016GL070695, 2016.

Pinder, R. W., Adams, P. J., Pandis, S. N., and Gilliland, A. B.: Temporally resolved ammonia emission inventories: current estimates, evaluation tools, and measurement needs, J. Geophys. Res.-Atmos., 111, 1984–2012, 2006.

Qu, Z., Henze, D. K., Capps, S. L., Wang, Y., Xu, X., and Wang, J.: Monthly top-down NO$_x$ emissions for China (2005–2012): a hybrid inversion method and trend analysis, J. Geophys. Res., 122, 4600–4625, https://doi.org/10.1002/2016JD025852, 2017.

Sacks, W. J., Deryng, D., Foley, J. A., and Ramankutty, N.: Crop planting dates: an analysis of global patterns, Global Ecol. Biogeogr., 19, 607–620, 2010.

SAGE (Sustainability and the Global Environment): University of Wisconsin, available at: https://nelson.wisc.edu/sage/data-and-models/atlas/maps.php (last access: December 2015), 2015.

Shephard, M. W. and Cady-Pereira, K. E.: Cross-track Infrared Sounder (CrIS) satellite observations of tropospheric ammonia, Atmos. Meas. Tech., 8, 1323–1336, https://doi.org/10.5194/amt-8-1323-2015, 2015.

Shephard, M. W., Cady-Pereira, K. E., Luo, M., Henze, D. K., Pinder, R. W., Walker, J. T., Rinsland, C. P., Bash, J. O., Zhu, L., Payne, V. H., and Clarisse, L.: TES ammonia retrieval strategy and global observations of the spatial and seasonal variability of ammonia, Atmos. Chem. Phys., 11, 10743–10763, https://doi.org/10.5194/acp-11-10743-2011, 2011.

Søgaard, H. T., Sommer, S. G., Hutchings, N. J., Huijsmans, J. F. M., Bussink, D. W., and Nicholson, F.: Ammonia volatilization from field-applied animal slurry – the ALFAM model, Atmos. Environ., 36, 3309–3319, https://doi.org/10.1016/S1352-2310(02)00300-X, 2002.

Stevens, C. J., Dise, N. B., Mountford, J. O., and Gowing, D. J.: Impact of nitrogen deposition on the species richness of grasslands, Science, 303, 1876–1879, 2004.

Streets, D. G., Bond, T. C., Carmichael, G. R., Fernandes, S. D., Fu, Q., He, D., Klimont, Z., Nelson, S. M., Tsai, N. Y., Wang, M. Q., Woo, J. H., and Yarber, K. F.: An inventory of gaseous and primary aerosol emissions in Asia in the year 2000, J. Geophys. Res.-Atmos., 108, 8809, https://doi.org/10.1029/2002JD003093, 2003.

Sun, K., Tao, L., Miller, D. J., Pan, D., Golston, L. M., Zondlo, M. A., Griffin, R. J., Wallace, H. W., Leong, Y. J., Yang, M. M., Zhang, Y., Mauzerall, D. L., and Zhu, T.: Vehicle emissions as an important urban ammonia source in the United States and China, Environ. Sci. Technol., 51, 2472–2481, https://doi.org/10.1021/acs.est.6b02805, 2017.

Teng, X., Hu, Q., Zhang, L., Qi, J., Shi, J., Xie, H., Gao, H., and Yao, X.: Identification of major sources of atmospheric NH$_3$ in an urban environment in northern China during wintertime, Environ. Sci. Technol., 51, 6839–6848, https://doi.org/10.1021/acs.est.7b00328, 2017.

Van Damme, M., Clarisse, L., Dammers, E., Liu, X., Nowak, J. B., Clerbaux, C., Flechard, C. R., Galy-Lacaux, C., Xu, W., Neuman, J. A., Tang, Y. S., Sutton, M. A., Erisman, J. W., and Coheur, P. F.: Towards validation of ammonia (NH$_3$) measurements from the IASI satellite, Atmos. Meas. Tech., 8, 1575–1591, https://doi.org/10.5194/amt-8-1575-2015, 2015.

van Donkelaar, A., Martin, R. V., Leaitch, W. R., Macdonald, A. M., Walker, T. W., Streets, D. G., Zhang, Q., Dunlea, E. J., Jimenez, J. L., Dibb, J. E., Huey, L. G., Weber, R., and Andreae, M. O.: Analysis of aircraft and satellite measurements from the Intercontinental Chemical Transport Experiment (INTEX-B) to quantify long-range transport of East Asian sulfur to Canada, Atmos. Chem. Phys., 8, 2999–3014, https://doi.org/10.5194/acp-8-2999-2008, 2008.

Wang, G., Zhang, R., Gomez, M. E., Yang, L., Levy Zamora, M., Hu, M., Lin, Y., Peng, J., Guo, S., Meng, J., Li, J., Cheng, C., Hu, T., Ren, Y., Wang, Y., Gao, J., Cao, J., An, Z., Zhou, W., Li, G., Wang, J., Tian, P., Marrero-Ortiz, W., Secrest, J., Du, Z., Zheng, J., Shang, D., Zeng, L., Shao, M., Wang, W., Huang, Y., Wang, Y., Zhu, Y., Li, Y., Hu, J., Pan, B., Cai, L., Cheng, Y., Ji, Y., Zhang, F., Rosenfeld, D., Liss, P. S., Duce, R. A., Kolb, C. E., and Molina, M. J.: Persistent sulfate formation from London Fog to Chinese haze, P. Natl. Acad. Sci. USA, 113, 13630–13635, https://doi.org/10.1073/pnas.1616540113, 2016.

Wang, J., Hoffmann, A. A., Park, R. J., Jacob, D. J., and Martin, S. T.: Global distribution of solid and aqueous sulfate aerosols: effect of the hysteresis of particle phase transitions, J. Geophys. Res., 113, D11206, https://doi.org/10.1029/2007jd009367, 2008.

Wang, Q., Jacob, D. J., Fisher, J. A., Mao, J., Leibensperger, E. M., Carouge, C. C., Le Sager, P., Kondo, Y., Jimenez, J. L., Cubison, M. J., and Doherty, S. J.: Sources of carbonaceous aerosols and deposited black carbon in the Arctic in winter-spring: implications for radiative forcing, Atmos. Chem. Phys., 11, 12453–12473, https://doi.org/10.5194/acp-11-12453-2011, 2011.

Wang, S. W., Liao, Q. J. H., Hu, Y. T., and Yan, X. Y.: A preliminary inventory of NH$_3$-N emission and its temporal and spatial distribution of China, Journal of Agro-Environment Science, 28, 619–626, 2009 (in Chinese with English abstract).

Wang, Y., Zhang, Q. Q., He, K., Zhang, Q., and Chai, L.: Sulfate-nitrate-ammonium aerosols over China: response to 2000–2015 emission changes of sulfur dioxide, nitrogen oxides, and ammonia, Atmos. Chem. Phys., 13, 2635–2652, https://doi.org/10.5194/acp-13-2635-2013, 2013.

Wang, Y. X., McElroy, M. B., Jacob, D. J., and Yantosca, R. M.: A nested grid formulation for chemical transport over Asia: applications to CO, J. Geophys. Res., 109, D22307, https://doi.org/10.1029/2004jd005237, 2004.

Warner, J. X., Wei, Z., Strow, L. L., Dickerson, R. R., and Nowak, J. B.: The global tropospheric ammonia distribution as seen in the 13-year AIRS measurement record, Atmos. Chem. Phys., 16, 5467–5479, https://doi.org/10.5194/acp-16-5467-2016, 2016.

Warner, J. X., Dickerson, R. R., Wei, Z., Strow, L. L., Wang, Y., and Liang, Q.: Increased atmospheric ammonia over the world's major agricultural areas detected from space, Geophys. Res. Lett., 44, 2875–2884, https://doi.org/10.1002/2016GL072305, 2017.

Wesely, M. L.: Parameterization of surface resistances to gaseous dry deposition in regional-scale numerical-models, Atmos. Environ., 23, 1293–1304, 1989.

Xu, P., Liao, Y. J., Lin, Y. H., Zhao, C. X., Yan, C. H., Cao, M. N., Wang, G. S., and Luan, S. J.: High-resolution inventory of ammonia emissions from agricultural fertilizer in China from 1978 to 2008, Atmos. Chem. Phys., 16, 1207–1218, https://doi.org/10.5194/acp-16-1207-2016, 2016.

Xu, W., Luo, X. S., Pan, Y. P., Zhang, L., Tang, A. H., Shen, J. L., Zhang, Y., Li, K. H., Wu, Q. H., Yang, D. W., Zhang, Y. Y., Xue, J., Li, W. Q., Li, Q. Q., Tang, L., Lu, S. H., Liang, T., Tong, Y. A., Liu, P., Zhang, Q., Xiong, Z. Q., Shi, X. J., Wu, L. H., Shi, W. Q., Tian, K., Zhong, X. H., Shi, K., Tang, Q. Y., Zhang, L. J., Huang, J. L., He, C. E., Kuang, F. H., Zhu, B., Liu, H., Jin, X., Xin, Y. J., Shi, X. K., Du, E. Z., Dore, A. J., Tang, S., Collett Jr., J. L., Goulding, K., Sun, Y. X., Ren, J., Zhang, F. S., and Liu, X. J.: Quantifying atmospheric nitrogen deposition through a nationwide monitoring network across China, Atmos. Chem. Phys., 15, 12345–12360, https://doi.org/10.5194/acp-15-12345-2015, 2015.

Yan, X., Akimoto, H., and Ohara, T.: Estimation of nitrous oxide, nitric oxide and ammonia emissions from croplands in East, Southeast and South Asia, Glob. Change Biol., 9, 1080–1096, https://doi.org/10.1046/j.1365-2486.2003.00649.x, 2003.

Yang, F., Tan, J., Zhao, Q., Du, Z., He, K., Ma, Y., Duan, F., Chen, G., and Zhao, Q.: Characteristics of $PM_{2.5}$ speciation in representative megacities and across China, Atmos. Chem. Phys., 11, 5207–5219, https://doi.org/10.5194/acp-11-5207-2011, 2011.

Zhang, L., Gong, S., Padro, J., and Barrie, L.: A size-segregated particle dry deposition scheme for an atmospheric aerosol module. Atmos. Environ., 35, 549–560, 2001.

Zhang, L., Jacob, D. J., Liu, X., Logan, J. A., Chance, K., Eldering, A., and Bojkov, B. R.: Intercomparison methods for satellite measurements of atmospheric composition: application to tropospheric ozone from TES and OMI, Atmos. Chem. Phys., 10, 4725–4739, https://doi.org/10.5194/acp-10-4725-2010, 2010.

Zhang, L., Jacob, D. J., Knipping, E. M., Kumar, N., Munger, J. W., Carouge, C. C., van Donkelaar, A., Wang, Y. X., and Chen, D.: Nitrogen deposition to the United States: distribution, sources, and processes, Atmos. Chem. Phys., 12, 4539–4554, https://doi.org/10.5194/acp-12-4539-2012, 2012.

Zhang, L., Liu, L., Zhao, Y., Gong, S., Zhang, X., Henze, D. K., Capps, S. L., Fu, T.-M., Zhang, Q., and Wang, Y.: Source attribution of particulate matter pollution over North China with the adjoint method, Environ. Res. Lett., 10, 084011, https://doi.org/10.1088/1748-9326/10/8/084011, 2015.

Zhang, L., Shao, J., Lu, X., Zhao, Y., Hu, Y., Henze, D. K., Liao, H., Gong, S., and Zhang, Q.: Sources and processes affecting fine particulate matter pollution over North China: an adjoint analysis of the Beijing APEC period, Environ. Sci. Technol., 50, 8731–8740, https://doi.org/10.1021/acs.est.6b03010, 2016.

Zhang, Q., Streets, D. G., Carmichael, G. R., He, K. B., Huo, H., Kannari, A., Klimont, Z., Park, I. S., Reddy, S., Fu, J. S., Chen, D., Duan, L., Lei, Y., Wang, L. T., and Yao, Z. L.: Asian emissions in 2006 for the NASA INTEX-B mission, Atmos. Chem. Phys., 9, 5131–5153, https://doi.org/10.5194/acp-9-5131-2009, 2009.

Zhang, W. F. and Zhang, F. S.: Report on the Development of Fertilizer in China, China Agriculture University Press, China, 2012 (in Chinese).

Zhang, Y., Dore, A. J., Ma, L., Liu, X. J., Ma, W. Q., Cape, J. N., and Zhang, F. S.: Agricultural ammonia emissions inventory and spatial distribution in the North China Plain, Environ. Pollut., 158, 490–501, https://doi.org/10.1016/j.envpol.2009.08.033, 2010.

Zhang, Y. S., Luan, S. J., Chen, L. L., and Shao, M.: Estimating the volatilization of ammonia from synthetic nitrogenous fertilizers used in China, J. Environ. Manage., 92, 480–493, https://doi.org/10.1016/j.jenvman.2010.09.018, 2011.

Zhao, B., Wang, S. X., Wang, J. D., Fu, J. S., Liu, T. H., Xu, J. Y., Fu, X., and Hao, J. M.: Impact of national NO_x and SO_2 control policies on particulate matter pollution in China, Atmos. Environ., 77, 453–463, https://doi.org/10.1016/j.atmosenv.2013.05.012, 2013.

Zhao, Y., Zhang, L., Pan, Y., Wang, Y., Paulot, F., and Henze, D. K.: Atmospheric nitrogen deposition to the northwestern Pacific: seasonal variation and source attribution, Atmos. Chem. Phys., 15, 10905–10924, https://doi.org/10.5194/acp-15-10905-2015, 2015.

Zhao, Y., Zhang, L., Chen, Y., Liu, X., Xu, W., Pan, Y., and Duan, L.: Atmospheric nitrogen deposition to China: a model analysis on nitrogen budget and critical load exceedance, Atmos. Environ., 153, 32–40, 2017.

Zhu, L., Henze, D. K., Cady-Pereira, K. E., Shephard, M. W., Luo, M., Pinder, R. W., Bash, J. O., and Jeong, G. R.: Constraining U.S. ammonia emissions using TES remote sensing observations and the GEOS-Chem adjoint model, J. Geophys. Res.-Atmos., 118, 3355–3368, 2013.

Zhu, L., Henze, D., Bash, J., Jeong, G.-R., Cady-Pereira, K., Shephard, M., Luo, M., Paulot, F., and Capps, S.: Global evaluation of ammonia bidirectional exchange and livestock diurnal variation schemes, Atmos. Chem. Phys., 15, 12823–12843, https://doi.org/10.5194/acp-15-12823-2015, 2015.